Retrievals of atmospheric CO_2 from simulated space-borne measurements of backscattered near-infrared sunlight: accounting for aerosol effects

André Butz,* Otto P. Hasekamp, Christian Frankenberg, and Ilse Aben

SRON Netherlands Institute for Space Research, Sorbonnelaan 2, 3584 CA Utrecht, The Netherlands

*Corresponding author: a.butz@sron.nl

Received 17 March 2009; revised 22 May 2009; accepted 26 May 2009;
posted 28 May 2009 (Doc. ID 108889); published 10 June 2009

Retrievals of atmospheric carbon dioxide (CO_2) from space-borne measurements of backscattered near-infrared sunlight are hampered by aerosol and cirrus cloud scattering effects. We propose a retrieval approach that allows for the retrieval of a few effective aerosol parameters simultaneously with the CO_2 total column by parameterizing particle amount, height distribution, and microphysical properties. Two implementations of the proposed method covering different spectral bands are tested for an ensemble of simulated nadir observations for aerosol (and cirrus) loaded scenes over low- and mid-latitudinal land surfaces. The residual aerosol-induced CO_2 errors are mostly below 1% up to aerosol optical thickness 0.5. The proposed methods also perform convincing for scenes where cirrus clouds of optical thickness 0.1 overlay the aerosol. © 2009 Optical Society of America

OCIS codes: 010.0280, 010.1280, 010.1310, 120.6200, 290.1090.

1. Introduction

Recent satellite missions aim at measuring atmospheric abundances of carbon dioxide (CO_2) with high precision, high accuracy, and global coverage. The Greenhouse Gases Observing Satellite (GOSAT) [1] has been in orbit since 23 January 2009, while the Orbiting Carbon Observatory (OCO) [2] suffered from a launch failure on 24 February 2009. Both instruments have been designed to observe near-infrared sunlight backscattered by the Earth's surface and atmosphere. Such observations in the solar infrared spectral range provide high sampling sensitivity near the Earth's surface and thus, are particularly suitable for inferring sources and sinks of atmospheric CO_2 [2–4].

So far, knowledge about the atmospheric branch of the carbon cycle is mainly derived from ground-based *in situ* measurements by the CO_2 flask sampling networks. Although providing highly accurate atmospheric CO_2 records, ground-based networks intrinsically suffer from sparse geographic coverage. Satellite based near-infrared sounders sampling atmospheric CO_2 at high temporal and spatial resolution could bridge this gap, provided the measurements are precise and accurate enough. A series of studies [5–10] has shown that space-based measurements of the column integrated dry air mixing ratio of CO_2 (X_{CO_2}) have to achieve a precision of about 1% [out of roughly 380 parts in 10^6 (ppm)] on regional scales to improve over source-sink estimates based on the ground-based networks alone. Moreover, regional systematic biases as low as a few tenths of a ppm could jeopardize the benefit of satellite measurements for source-sink determination.

Light path modification due to scattering by aerosols and cirrus has been identified a major source of error when retrieving X_{CO_2} from solar near-infrared backscatter measurements [11–14]. In comparison to a reference lightpath, scattering events can have a

0003-6935/09/183322-15$15.00/0

lightpath enhancing or lightpath shortening effect depending on the scattering angles, scattering heights, and number of events occurring. The relative importance of the scattering effects with respect to the unperturbed lightpath is controlled by the surface albedo of the observed scene. Because of the homogeneous distribution of CO_2 throughout the atmosphere, unaccounted lightpath enhancement typically goes along with enhanced CO_2 absorption and, hence, overestimation of the CO_2 abundance, while unaccounted lightpath shortening yields underestimation of atmospheric CO_2. Hence, it is crucial for accurate CO_2 retrievals to take into account atmospheric scattering properties.

Several approaches have been suggested for how to account for aerosol (and cirrus) induced lightpath modification in CO_2 retrievals from satellite measurements [11,15–19]. These approaches adopt strategies such as the usage of prior information about atmospheric scattering properties, the retrieval of a lightpath proxy from absorption features of molecular oxygen (O_2), the direct retrieval of atmospheric scattering properties, or combinations of these. Oshchepkov *et al.* [19] propose to account for cirrus cloud scattering in GOSAT measurements by estimating parameters of the photon path length distribution. They conclude on residual X_{CO_2} errors of less than 1% for cirrus optical thickness up to 0.2. For OCO, Connor *et al.* [18] set up an algorithm that simultaneously retrieves the CO_2 vertical profile, surface pressure, and an aerosol vertical profile. An optimal estimation method constrains the heavily underdetermined problem to physically reasonable solutions by the use of *a priori* information. They investigated the impact of the limited information about the aerosol vertical profile on retrieved X_{CO_2} by a linear error analysis and concluded very small residual errors up to aerosol optical thickness 0.3. An important error source that is not considered, however, is the difference between the assumed and the true microphysical properties of aerosol and cirrus particles.

We propose an alternative approach that simultaneously retrieves the CO_2 total column and effective aerosol properties based on a simple aerosol microphysical model. The approach is tested for an ensemble of simulated observations that rely on an aerosol description that is inconsistent with the aerosol description used in the retrieval algorithm. For the retrieval simulations, we adopt the properties of the OCO instrument, which is regarded as a generic example for a near-infrared sounder that measures the relevant molecular absorption bands at high spectral resolution. Thus, our study is readily applicable to measurements of the Thermal and Near-Infrared Sensor for carbon Observation–Fourier Transform Spectrometer (TANSO-FTS) onboard GOSAT or any future OCO-like mission. We discuss two implementations of the proposed approach. The "3-band" retrieval exploits measurements of the O_2 A band at $0.77\,\mu$m and the CO_2 absorption bands at 1.61 and $2.06\,\mu$m to retrieve a parameter for the aerosol amount, a parameter characterizing the aerosol height distribution, and a parameter characterizing the aerosol size distribution. The "2 micron" retrieval uses the CO_2 absorption band at $2.06\,\mu$m and retrieves parameters for aerosol amount and aerosol height distribution, only. The conceptual difference between the two methods comes from their approximate treatment of aerosol optical properties. The "3-band" approach retrieves an aerosol size distribution parameter that controls the spectral variation of aerosol optical properties among the considered spectral bands. The "2 micron" retrieval does not retrieve such a parameter but assumes a prescribed dependence of aerosol optical properties on wavelength within the relatively narrow CO_2 absorption band around $2.06\,\mu$m.

We limit our study to nadir observations over land surfaces. Ocean and snow covered scenes are not considered. The trial ensemble of simulated measurements over aerosol loaded scenes is generated from output of a global aerosol model, thereby relying on a complex description of aerosol properties. Although cirrus clouds are not explicitly considered by the retrieval approach, the proposed methods are also tested for generic cirrus clouds overlaying the aerosol scenes. Our dedicated goal is to estimate the residual X_{CO_2} error induced by the simplifying aerosol treatment in the retrieval methods.

Sections 2 and 3 describe the retrieval and simulation methods, respectively. Section 4 discusses retrieval performance for the ensemble of trial spectra, and Section 5 concludes this study.

2. Retrieval Method

Any retrieval method aims at inferring the state vector $\mathbf{x}$ from the measurement vector $\mathbf{y}$. The state vector is linked to the measurement through the true forward model $\mathbf{f}(\mathbf{x},\mathbf{b})$ that depends on $\mathbf{x}$ and on ancillary parameters $\mathbf{b}$,

$$\mathbf{y} = \mathbf{f}(\mathbf{x},\mathbf{b}) + \boldsymbol{\epsilon}_y, \tag{1}$$

where $\boldsymbol{\epsilon}_y$ represents the measurement noise error. The retrieval method approximates $\mathbf{f}(\mathbf{x},\mathbf{b})$ by a retrieval forward model $\mathbf{F}(\mathbf{x},\mathbf{b})$ that imposes the retrieval forward model error $\boldsymbol{\epsilon}_F$ as additional error term:

$$\mathbf{y} = \mathbf{F}(\mathbf{x},\mathbf{b}) + \boldsymbol{\epsilon}_y + \boldsymbol{\epsilon}_F. \tag{2}$$

From Eq. (2), we seek the state vector $\hat{\mathbf{x}}$ by minimizing the least-squares cost function

$$\hat{\mathbf{x}} = \arg\min_{\mathbf{X}} \left(||\mathbf{S}_\mathbf{y}^{-\frac{1}{2}}(\mathbf{F}(\mathbf{x},\mathbf{b}) - \mathbf{y})||^2 \right), \tag{3}$$

where $\mathbf{S}_\mathbf{y}$ is the measurement error covariance matrix. Since the forward model $\mathbf{F}(\mathbf{x},\mathbf{b})$ is nonlinear in $\mathbf{x}$, the minimization problem is solved iteratively in linear approximation by a Levenberg–Marquardt algorithm. The iteration is terminated when the

update of the state vector is negligible in comparison to the required accuracy.

Here, we aim at estimating the effect of the retrieval forward model error $\boldsymbol{\epsilon}_F$ on inferred X_{CO_2} caused by the approximate treatment of aerosols (and cirrus) in the retrieval forward model. To this end, we simulate measurements by a simulation forward model $\mathbf{f}(\mathbf{x},\mathbf{b})$ (Section 3) which relies on a sophisticated description of aerosol and cirrus effects. Retrievals are performed by the approximate retrieval forward model $\mathbf{F}(\mathbf{x},\mathbf{b})$ (Subsection 2.B) under noiseless conditions ($\boldsymbol{\epsilon}_y = 0$) implying that the residual error on X_{CO_2} imposed by $\boldsymbol{\epsilon}_F$ is given by the difference between the true and the retrieved state vector. For our noiseless retrievals, the measurement error covariance $\mathbf{S}_y$ is only used for weighting the least-squares cost function according to Eq. (3).

A. Measurements

The measurements are spectra of sunlight backscattered by the Earth's surface and atmosphere to a space-borne observer. We define the components y_i of the measurement vector $\mathbf{y}$ as the logarithm of the corresponding intensity recorded by detector pixel i. Considering the definition of $\mathbf{y}$ as logarithmic intensity, the measurement error covariance matrix $\mathbf{S}_y$ is calculated assuming that the signal-to-noise of the detected intensity is 500, 300, 150 in the continuum of the O_2 A band, the weak, and the strong CO_2 band, respectively. Within each absorption band, noise scales with the square root of intensity, implying that shot noise is the dominating noise contribution. We assume that only the polarization direction perpendicular to the reference plane spanned by the Sun, the satellite observer, and the reflection point at the Earth's surface is detected. Three spectral windows are considered: the O_2 A band ([0.757 μm, 0.775 μm]) and a weakly and a strongly absorbing CO_2 band ([1.594 μm, 1.627 μm]; [2.043 μm, 2.087 μm]). The instrument line shape is given by a Gaussian with full width at half-maximum (FWHM) of 0.042 nm at the O_2 A band, 0.076 nm at the weak CO_2 band, and 0.097 nm at the strong CO_2 band. Figure 1 shows exemplary spectra of the covered spectral bands. The "3-band" retrieval uses all three spectral bands, while the "2 micron" retrieval only considers the strongly absorbing CO_2 band around 2.06 μm. The two approaches are compared to a "nonscattering" retrieval, which neglects any scattering in the atmosphere and only uses the weakly absorbing CO_2 band around 1.61 μm.

B. Forward Model and State Vector

The core of the forward model $\mathbf{F}(\mathbf{x},\mathbf{b})$ is the vector radiative transfer model (RTM) developed by Hasekamp and Landgraf [20,21]. Given input by the state vector $\mathbf{x}$ and the auxiliary parameters $\mathbf{b}$, the RTM calculates the Stokes vector of solar radiation backscattered to space by the Earth's surface and atmosphere considering molecular and particulate absorption as well as multiple scattering by molecules and particles in a multilayer, inhomogeneous, plane-parallel atmosphere. The RTM also provides the derivatives of the Stokes vector with respect to absorption and scattering optical thickness, scattering phase matrix, and surface albedo from which the derivatives with respect to the state vector elements can be inferred via the chain rule for differentiation. The RTM has been employed successfully for trace gas as well as aerosol and cloud property retrievals in a variety of studies [20,22,23]. A newly developed linear-k approach avoids computationally expensive line-by-line calculations by binning monochromatic calculations [24].

Here, the forward model considers 36 atmospheric layers with boundaries equidistant in pressure. Surface reflectance is parameterized by a scalar Lambertian albedo. Molecular absorption cross sections are calculated from the latest spectroscopic databases [25,26] assuming Voigt lineshapes. Spectral gridding is equidistant in wavelength with 0.001 nm grid spacing in the O_2 A band and a 0.002 nm grid spacing in the CO_2 bands. The solar irradiance is set to unity. Spectral resolution of the generic OCO-like instrument is considered by convolving the modeled radiance spectra and the corresponding derivatives with a Gaussian instrument function as described in Subsection 2.A.

Aerosol optical properties, i.e., the aerosol scattering and absorption optical thickness and the aerosol scattering phase matrix, are derived from input aerosol physical properties applying Mie theory under

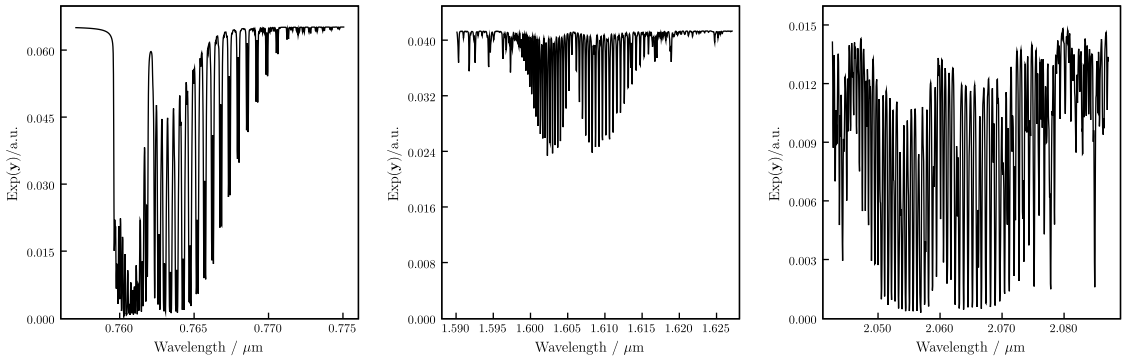

Fig. 1. Exemplary spectra of the O_2 A band (left panel), the weakly absorbing CO_2 band (middle panel), and the strongly absorbing CO_2 band (right panel). Spectra are modeled for a grass surface observed at nadir and solar zenith angle 30°.

the assumption that the aerosols are of spherical shape [21,27,28]. Physical input parameters are the aerosol total column number density N_{aer}, the aerosol size distribution $n_{\mathrm{aer}}(r)$, and the aerosol real and imaginary refractive index, m_r and m_i, which are assumed independent of wavelength within a retrieval window. For $n_{\mathrm{aer}}(r)$, we use a power-law size distribution according to [29]

$$n_{\mathrm{aer}}(r) = \begin{cases} A, & r \le r_1 \\ A(r/r_1)^{-\alpha}, & r_1 < r \le r_2 \\ 0, & r > r_2, \end{cases} \qquad (4)$$

where r is the particle radius, $r_1 = 0.1\,\mu$m, $r_2 = 10\,\mu$m, and the constant A is determined from normalization of the size distribution. Figure 2 illustrates the power-law size distribution and compares it to multimodal lognormal size distributions as used for testing the retrieval method (Section 3). Through its parameter α, the aerosol size distribution controls the spectral dependence of aerosol optical properties among the considered retrieval windows. Given N_{aer}, $n_{\mathrm{aer}}(r)$, m_r, and m_i, we calculate the scattering and absorption aerosol optical thickness integrated along the vertical from the top of the atmosphere to the ground, $\tau_{\mathrm{aer,sca}}$ and $\tau_{\mathrm{aer,abs}}$, and the aerosol scattering phase matrix. We define the total aerosol vertical optical thickness $\tau_{\mathrm{aer}} = \tau_{\mathrm{aer,sca}} + \tau_{\mathrm{aer,abs}}$, which we simply refer to as aerosol optical thickness in the following.

The height distribution of aerosols is parameterized by a generic function $h(z_k)$ such that the aerosol optical thickness in layer k at height z_k and depth Δz_k is given by

$$\tau_{\mathrm{aer},k} = \tau_{\mathrm{aer}} h(z_k) \Delta z_k, \qquad (5)$$

where $h(z_k)\Delta z_k$ is normalized to 1 when summing over all layers. We choose $h(z_k)$, a Gaussian function

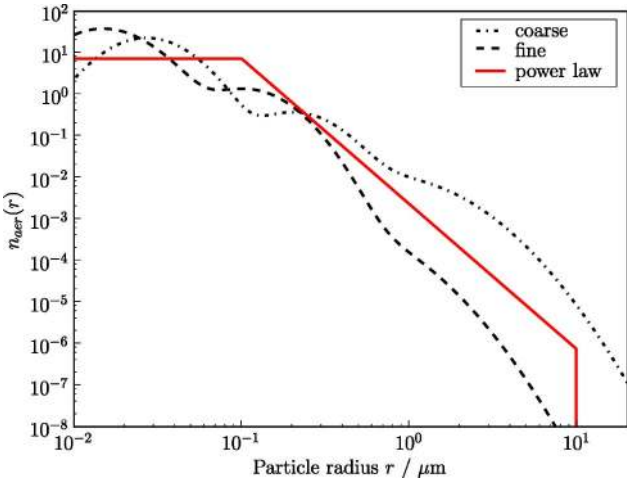

Fig. 2. (Color online) Aerosol size distribution $n_{\mathrm{aer}}(r)$ as a function of particle radius r. The retrieval methods rely on a power law (solid) size distribution. Multimodal lognormal size distributions such as shown for a fine (dashed) and a coarse (black dotted) particle aerosol are used for testing the retrieval approaches.

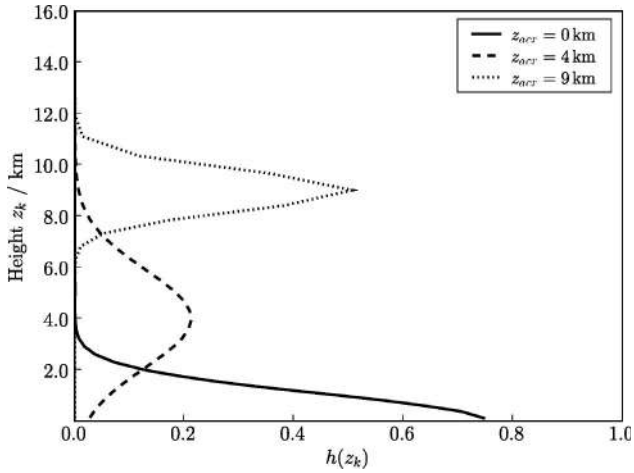

Fig. 3. Gaussian height distributions $h(z_k)$ for different center heights z_{aer} as adopted for the retrieval methods.

of center height z_{aer} and width $w_{\mathrm{aer}}(z_{\mathrm{aer}})$:

$$h(z_k) = A \exp\left[-\frac{4 \ln 2 (z_k - z_{\mathrm{aer}})^2}{w_{\mathrm{aer}}(z_{\mathrm{aer}})^2}\right], \qquad (6)$$

$$w_{\mathrm{aer}}(z_{\mathrm{aer}}) = w_0 \exp\left[-\frac{4 \ln 2 (z_{\mathrm{aer}} - w_0)^2}{(2w_0)^2}\right], \qquad (7)$$

with $w_0 = 4\,$km. This parameterization is designed to represent a well-confined boundary layer or elevated aerosol layer, or a broad aerosol layer in the free troposphere as illustrated by Fig. 3.

The above description of the forward model applies to the "3-band" and "2 micron" methods. For the "nonscattering" retrieval, only molecular absorption and reflection of sunlight at the Earth's surface are considered, i.e., absorption and scattering by aerosols as well as scattering by molecules is neglected.

The definition of the state vector $\mathbf{x}$ differs for the three retrieval approaches. Common state vector elements are the CO_2 total column, the H_2O total column, and surface albedo and its first order spectral dependence for each considered retrieval window. The "nonscattering" retrieval assumes no additional retrieval parameters. The "3-band" retrieval additionally retrieves three aerosol parameters, which are the aerosol total column number density N_{aer}, the size distribution parameter α, and the aerosol height distribution parameter z_{aer}. The "2 micron" retrieval includes two aerosol parameters in the state vector, in addition to the common state vector elements, the aerosol total column number density N_{aer}, and the aerosol height distribution parameter z_{aer}. Auxiliary nonretrieved parameters $\mathbf{b}$ comprise parameters such as the atmospheric pressure and temperature profiles and the spectroscopic parameters describing CO_2 and H_2O absorption. Further, for the "3-band" and "2 micron" retrieval, the aerosol real and imaginary refractive index are prescribed in

the forward model. For the "2 micron" retrieval, also the aerosol size distribution parameter α is a nonretrieved forward model parameter.

The target quantity X_{CO_2} is calculated from the retrieved CO_2 total column and surface pressure. Despite its direct impact on X_{CO_2}, topographically averaged surface pressure is not retrieved but assumed known with sufficient accuracy from meteorological and topographic support data. Further, we limit the retrieval to a total column CO_2 retrieval and do not attempt to retrieve a multilayer CO_2 vertical profile, since our goal here is to assess the accuracy of the proposed aerosol treatment in the forward model and, hence, we assume that the CO_2 profile shape is known. The same holds for the vertical profiles of H_2O, pressure, and temperature. Clearly, retrieval accuracy can suffer from inaccurate knowledge of the meteorological variables and vertical profile shapes. However, these sources of error are not studied here.

The treatment of aerosols in the proposed forward model is highly simplified in comparison to the true variability of aerosol types, sizes, and height distributions and, hence, can only be an effective description for the impact of atmospheric particles on CO_2 retrievals. Albeit not being explicitly designed for it, the proposed retrieval method is intended to also account to some extent for the effect of cirrus particles that exhibit optical properties significantly different from Mie particles. During the development of the retrieval algorithm, several options were tested for how to represent atmospheric particles in the retrieval forward model. More realistic aerosol models with multiple state vector elements for aerosol refractive indices, height, and size distributions or models including aerosol and cirrus type particles yielded unsatisfactory results. Typically, the least-squares inverse method did not converge since the measurements did not contain enough information on the state vector elements. Essentially, the proposed approach to retrieve a small number of parameters of a simple aerosol model is a trade-off between stability of the retrieval and minimizing the retrieval error due to simplified representation of aerosol and cirrus properties. Quantifying this retrieval bias is the subject of Section 4.

3. Simulation Method

The simplified treatment of aerosols in the retrieval method introduces an error on the target quantity X_{CO_2} when the retrieval is applied to true atmospheric spectra. To quantify the aerosol (and cirrus) induced retrieval error, an ensemble of simulated radiance spectra has to be generated by a simulation forward model $\mathbf{f}(\mathbf{x}, \mathbf{b})$ that is able to cover and to realistically model the range of scenes encountered in prospective satellite measurements.

A. Aerosol Ensemble Simulation

For our purposes, it is natural to use the forward model described in Subsection 2.B for generating the aerosol loaded trial spectra but to replace the aerosol model by a more sophisticated approach that can catch the variability of atmospheric aerosols.

The refined aerosol model again relies on Mie theory to calculate aerosol scattering optical thickness, aerosol absorption optical thickness, and aerosol scattering phase matrix from the aerosol total column number density $N_{\mathrm{aer},s}$, the size distribution $n_{\mathrm{aer},s}(r)$, and the real and imaginary refractive index, $m_{r,s}$ and $m_{i,s}$, where the subscript s represents quantities used for the simulations. Refractive indices are assumed independent of wavelength within the retrieval windows. The aerosol size distribution is a superposition of seven lognormal size distributions [30]:

$$n_{\mathrm{aer},s}(r) = \sum_{i=1}^{7} \frac{f_i}{\sqrt{2\pi}\sigma_i} \frac{1}{r} \exp\left[-\frac{(\ln r - \ln r_i)^2}{2\sigma_i^2}\right], \qquad (8)$$

where r is the particle radius, f_i is the mode fraction of mode i, and r_i and σ_i are the characteristic radius and width of mode i. Superpositions of lognormal size distributions are widely used when measuring and modeling atmospheric aerosols [31,32]. Figure 2 illustrates typical aerosol size distributions used for this study. The height distribution of aerosol optical thickness is not constrained by a generic function as for the proposed retrieval methods. Rather, we specify aerosol microphysical properties and thus aerosol optical properties individually for each atmospheric layer.

Aerosol input parameters for the ensemble simulations come from a run of the global aerosol model ECHAM5-HAM [32]. We use a model run for the year 2015 according to the A1B scenario defined by the Intergovernmental Panel on Climate Change (IPCC) [33], which was readily available from previous studies. ECHAM5-HAM provides estimates of aerosol particle number concentrations and size distribution parameters for seven modes of a lognormal size distribution in 19 atmospheric layers between the ground and 10 hPa pressure on a ~3° by ~3° latitude by longitude grid. The aerosol modes are identifiable as nucleation soluble, Aitken soluble, accumulation soluble, coarse soluble, Aitken insoluble, accumulation insoluble, and coarse insoluble. Each mode is a composite of five aerosol chemical types, i.e., sulfate, black carbon, organic matter, sea salt, and mineral dust. Details on the ECHAM5-HAM model and validation studies for the modeled aerosol abundances can be found in Stier *et al.* [32]. For each mode and considered spectral window, we calculate an average refractive index weighted by the relative mass contribution of the individual aerosol chemical type. The various aerosol size modes are considered through Eq. (8). Given size distribution and modewise refractive indices, aerosol scattering and the absorption optical thickness and the aerosol scattering phase matrix are computed for the 19 ECHAM5-

HAM layers individually and then interpolated to the simulation forward model height grid.

The members of our trial ensemble are chosen out of ECHAM5-HAM model output with the intention to cover the range of aerosol-surface scenes encountered by a space-borne observer. Since we focus on testing our retrievals for typical scenarios, less emphasis is put on selecting the scenes according to their true occurrence frequency. Because of the high computational cost, processing an ensemble that is truly representative of the global aerosol distribution in time and space would exceed the scope of this study. We pick the ensemble members from a winter and a summer day out of a global map of modeled aerosol data where we only consider locations with less than 500 m surface elevation, since we target at implications for the full atmospheric CO_2 column. Further, we only consider land surfaces at low- and mid-latitudes (latitude $<68°$) to avoid very low surface albedo, such as encountered for ocean surfaces throughout the near-infrared and for snow-covered surfaces in the considered CO_2 bands. For such surface scenes, retrieval performance typically is poor and not considered any further.

We scale the modeled aerosol optical thickness for individual scenes such that we obtain a good ensemble coverage up to aerosol optical thickness 0.5 (at $0.77\,\mu$m) resulting in an ensemble median aerosol optical thickness of 0.13 (at $0.77\,\mu$m). Scenes with aerosol optical thickness greater than 0.5 (at $0.77\,\mu$m) are not considered. Figure 4 illustrates the occurrence of $\tau_{\mathrm{aer},s}(0.77\,\mu\mathrm{m})$ in bins of 0.05 among the ~700 considered ensemble members. A histogram of the Ångstrom coefficient β is shown in Fig. 5, indicating that the ensemble covers a wide range of aerosol types and sizes, in particular coarse and fine aerosols. The Ångstrom coefficient β is a measure for the spectral dependence of the aerosol optical thickness and calculated through

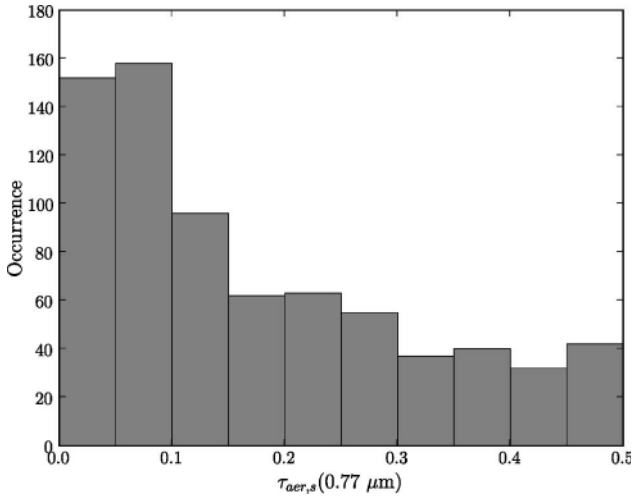

Fig. 4. Histogram of the aerosol optical thickness $\tau_{\mathrm{aer},s}(0.77\,\mu\mathrm{m})$ for the trial ensemble.

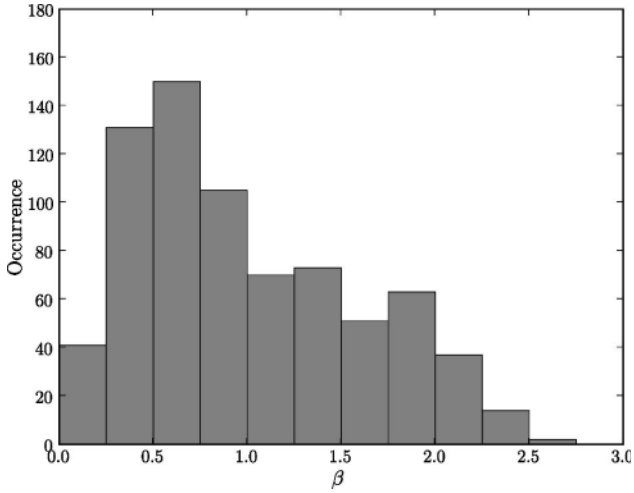

Fig. 5. Histogram of the Ångstrom coefficient β for the trial ensemble.

$$\frac{\tau_{\mathrm{aer},s}(\lambda_1)}{\tau_{\mathrm{aer},s}(\lambda_2)} = \left(\frac{\lambda_1}{\lambda_2}\right)^{-\beta}, \tag{9}$$

where λ_1 and λ_2 indicate different wavelengths. Here, we used a least-squares fit among the center wavelengths of the three considered spectral windows to estimate β. The vertically integrated single-scattering albedo, calculated from vertically integrated scattering and absorption optical thickness, ranges between 0.87 and 0.99 among our aerosol ensemble. For individual atmospheric layers, single-scattering albedo can be significantly lower. Figure 6 shows the modeled height distributions of aerosol optical thickness. ECHAM5-HAM covers boundary layer type aerosols, extended aerosol layers in the troposphere, as well as elevated aerosols in the upper troposphere and stratosphere. In particular, the considered height distributions do

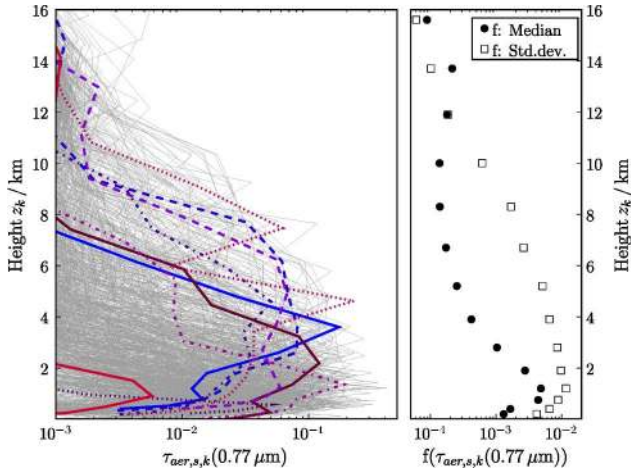

Fig. 6. (Color online) Left panel: aerosol optical thickness $\tau_{\mathrm{aer},s,k}$ in layer k as a function of layer height z_k considered by the trial ensemble. Exemplary individual profiles are shown in blue and red online. Right panel: median (full circles) and standard deviation (open squares) of aerosol optical thickness $\tau_{\mathrm{aer},s,k}$ in layer k among the trial ensemble.

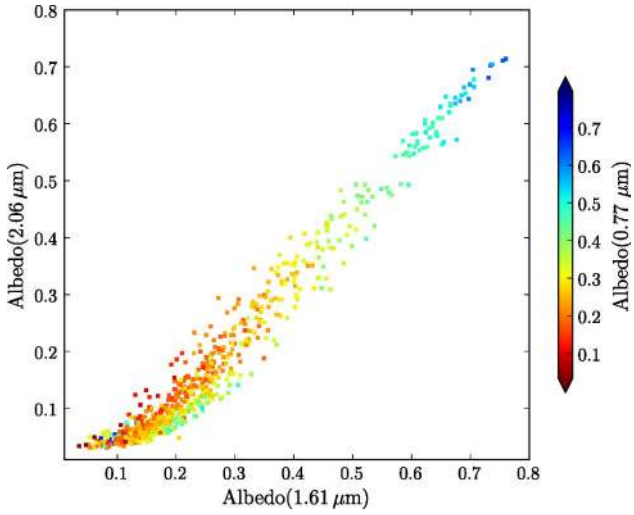

Fig. 7. (Color online) Surface albedo considered by the trial ensemble. The color scale shows albedo for the O_2 A band at 0.77 μm ranging from low (red online) to high (blue online). The scatter plot relates albedo at the two CO_2 bands.

not coincide with the generic Gaussian function of layer height implemented in the retrieval method.

ECHAM5-HAM model output comes with vertical profiles of pressure, temperature, and humidity, which are readily taken as input for the simulations and retrievals. The true CO_2 mixing ratio is set to 380 ppm throughout the atmosphere.

The surface albedo ensemble is assembled from the MODIS LAND albedo product available in 16 d bins on a 0.5 km by 0.5 km grid through http://lpdaac.usgs.gov/modis/mcd43a4v5.asp. We adopt MODIS band 2 (0.841 to 0.876 μm) albedo as the mean albedo in the O_2 A band, MODIS band 6 (1.628 to 1.652 μm) albedo as the mean albedo in the weak CO_2, and MODIS band 7 (2.105 to 2.155 μm) albedo as the mean albedo in the strong CO_2 band. Albedo data are selected for the center of the ECHAM5-HAM grid cell from a MODIS data bin in January and June 2007 for the winter and summer scenes, respectively. Figure 7 illustrates the ensemble of selected surface scenes. Surface albedo in the three spectral bands covers almost the whole range between 0 and 1. Grass, conifer, and deciduous surface types exhibit albedo between 0.2 and 0.4 in the O_2 A band with lower albedo in the CO_2 bands. Albedo as high as 0.5 to 0.7 throughout the near-infrared is characteristic for desert surfaces, while clay surfaces exhibit rather low albedo in the O_2 A band and albedo as high as 0.4 in the CO_2 bands. Cases with albedo as high as 0.8 in the O_2 A band and albedo as low as 0.05 in the CO_2 bands represent some residual snow covered scenes.

B. Generic Cirrus Simulations

Our retrieval method is designed to model the effect of aerosols on X_{CO_2} retrievals while cirrus clouds are not explicitly considered in the retrieval forward model. However, we expect the proposed "3-band" and "2 micron" retrieval approaches to be capable of modeling the effect of thin cirrus clouds to some extent. To estimate retrieval performance for cirrus-loaded scenes, we simulate generic cirrus clouds that overlay the ensemble of aerosol scenes described in Subsection 3.A.

The cirrus cloud model developed by Hess and Wiegner [34] and Hess [35] calculates the phase matrix and the scattering and absorption optical thickness of hexagonal ice crystals given a cirrus total column number density $N_{\mathrm{cir},s}$. The ice crystals are assumed to be randomly oriented in space and to exhibit columnar shape. With a being the length of the side of the hexagon and c being the length of the column, cirrus optical properties are computed for eight crystal size pairs (a,c) between (1.4 μm, 3.5 μm) and (110 μm, 1300 μm), essentially following Table 1 in Hess and Wiegner [34]. Since model calculations for perfect hexagonal ice crystals exhibit unrealistically pronounced halos of the phase matrix at 22° and 44° scattering angle, we apply a smoothing correction suggested by Hess [35]. Given the database of crystal size pairs (a,c), we aggregate cirrus optical properties according to a power-law size distribution $n_{\mathrm{cir},s}(c)$ in analogy to the study by Heymsfield and Platt [36] who inferred power-law size distributions for particles larger than 20 μm from their measurements:

$$n_{\mathrm{cir},s}(c) = \begin{cases} 0, & c \le c_1 \\ A(c/c_1)^{-3.85}, & c_1 < c \le c_2 \\ 0, & c > c_2, \end{cases} \qquad (10)$$

where we assume $c_1 = 3.5\,\mu$m and $c_2 = 1300\,\mu$m. The constant A is determined from normalization of the size distribution.

Our simulations here consider only purely crystalline cirrus clouds that contain the described type and size distribution of particles. We generate a cirrus trial ensemble by processing the aerosol ensemble described in Subsection 3.A and assuming an additional cirrus cloud of $\tau_{\mathrm{cir},s}(0.77\,\mu\mathrm{m}) = 0.1$ confined to a boxlike layer between 9 and 10 km.

4. Retrieval Exercises

The proposed retrieval methods are applied to the aerosol and cirrus trial ensemble. Our discussion focuses on the residual aerosol-induced retrieval error and its dependencies on aerosol and surface properties. Some implications are inferred for cirrus-loaded scenes.

The trial ensembles are processed for nadir viewing geometry (viewing zenith angle 0°) and solar zenith angles (SZA) 30° and 60°. The retrievals are launched with an initial guess that corresponds to the true values for the CO_2 and H_2O total columns and the albedo parameters to minimize the number of iterations. For the "3-band" retrieval, the initial aerosol optical thickness is $\tau_{\mathrm{aer}} = 0.15$ at 0.77 μm with an initial size distribution parameter $\alpha = 3.5$ according to Eq. (4), and an initial height distribution parameter $z_{\mathrm{aer}} = 3$ km according to Eq. (6). The corresponding initial aerosol optical thickness at

1.61 and 2.06 μm is 0.10 and 0.09, respectively. For the "2 micron" retrieval, the initial aerosol optical thickness is $\tau_{\mathrm{aer}} = 0.09$ at 2.06 μm with an initial height distribution parameter $z_{\mathrm{aer}} = 3$ km, while the aerosol size distribution parameter is fixed at $\alpha = 3.5$. Aerosol refractive indices for the "3-band" and "2 micron" retrievals are given by $m_r = 1.4$ and $m_i = -0.003$. The initial values for aerosol optical thickness, aerosol height distribution parameter z_{aer}, and aerosol size distribution parameter α are chosen *ad hoc* to roughly represent intermediate values for aerosol amount, height, and size. The refractive indices approximately correspond to the median column averaged refractive indices at 0.77 μm among the trial ensemble. We emphasize that it is inherently impossible to initialize the retrievals by the true aerosol parameters, since the true forward model $\mathbf{f}(\mathbf{x}, \mathbf{b})$ and the retrieval forward model $\mathbf{F}(\mathbf{x}, \mathbf{b})$ differ by their parameterization of aerosols and, hence, require physically different input parameters.

The retrievals are performed under noiseless conditions as pointed out in Section 2. Hence, the residual aerosol-induced retrieval error is simply given by the difference between retrieved $X_{\mathrm{CO_2}}$ and the true value of 380 ppm. When adding noise to the simulated trial spectra, the noise induced retrieval error has to be considered in addition, e.g., through linear error analysis [37]. Test retrievals for noisy spectra (continuum signal-to-noise: 500 in the O_2 A band, 300 in the weak CO_2 band, 150 in the strong CO_2 band) show that the inferred aerosol (and cirrus) induced retrieval errors are consistent with our derivations for noiseless trials. Typically, the residual spectral structures induced by the approximate aerosol forward model are well within the measurement noise.

A. Aerosol Ensemble Retrievals

Figures 8–10 show the residual aerosol-induced $X_{\mathrm{CO_2}}$ error when applying the proposed retrieval approaches to the aerosol trial ensemble. We show the residual $X_{\mathrm{CO_2}}$ error as a function of aerosol optical thickness at 0.77 μm (Fig. 8), surface albedo (Fig. 9), and the Ångstrom coefficient of the simulated aerosol burden (Fig. 10). The latter aims at illustrating error sensitivity to aerosol type and size. Typically, large aerosols imply smaller Ångstrom coefficients than small aerosols. We further

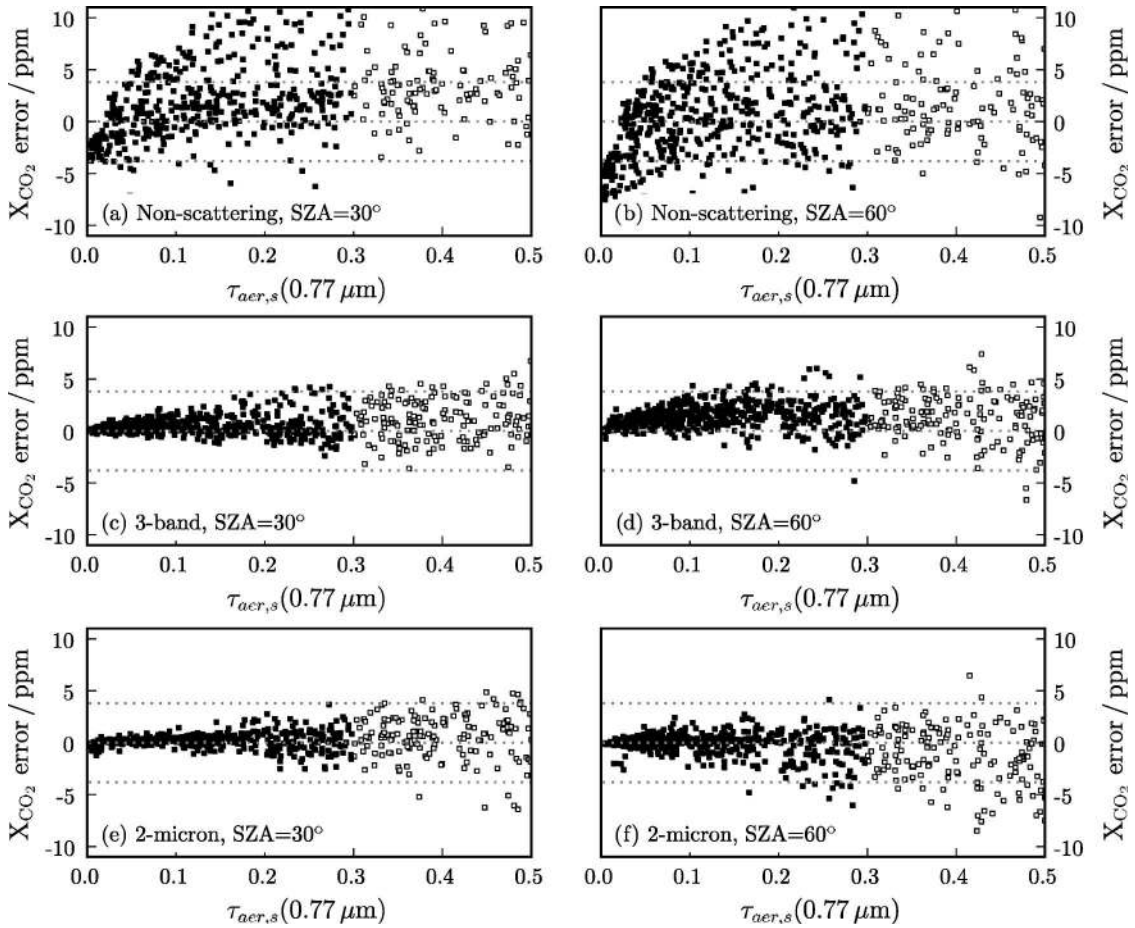

Fig. 8. Residual aerosol-induced $X_{\mathrm{CO_2}}$ error as a function of aerosol optical thickness at 0.77 μm for (a) and (b) "nonscattering" retrieval; (c) and (d) "3-band" retrieval; and (e) and (f) "2 micron" retrieval. Results are shown at SZA = 30° for (a), (c), and (e) and SZA = 60° for (b), (d), and (f). Filled and open boxes correspond to scenes with aerosol optical thickness less and greater than 0.3, respectively. Dotted gray lines indicate 1% error limits.

distinguish between cases with aerosol optical thickness less than 0.3 and greater than 0.3 (at 0.77 μm) since it is common for satellite-mission planning to foresee aerosol optical thickness 0.3 as the threshold for actually processing observations [2].

The results for the "nonscattering" approach illustrate that neglecting scattering yields X_{CO_2} retrieval errors that can be substantial [Figs. 8(a) and 8(b)]. Errors exceed 1% in many cases for aerosol optical thickness less than 0.3. Retrieval errors show a correlation with albedo where low albedo yields underestimation and high albedo overestimation of true X_{CO_2} in agreement with the findings of Aben *et al.* [14] [Figs. 9(a) and 9(b)]. There is a range of surface albedo around 0.2 (at 1.61 μm), where aerosols have a vanishing net effect on the "nonscattering" CO_2 retrievals. Further, we observe a trend to high X_{CO_2} retrievals for small Ångstrom coefficients and a trend to low X_{CO_2} retrievals for large Ångstrom coefficients [Figs. 10(a) and 10(b)]. Retrievals for SZA = 60° tentatively reveal more scatter and a larger spread of the residual error than retrievals for SZA = 30°. For vanishing aerosol optical thickness, the "nonscattering" retrievals are low-biased due to the neglect of Rayleigh scattering. The latter effect is particularly pronounced since for our ensemble low-aerosol optical thickness in a lot of cases coincides with low albedo where the Rayleigh scattered contribution to the observed radiance is significant.

In general, the errors observed for the "nonscattering" retrieval can be understood as a trade-off between lightpath-enhancing and lightpath-shortening effects of aerosols. These effects have been discussed in detail by others [14,38]. The "nonscattering" retrieval assumes a direct lightpath from the Sun to the space-borne observer via reflection at the Earth's surface. Any effect that shortens the true lightpath in comparison to the direct lightpath results in underestimation of true X_{CO_2} since a shorter lightpath relates to shallower CO_2 absorption lines, which in turn is interpreted as less atmospheric CO_2 abundance. In analogy, any lightpath-enhancing effect results in overestimation of true X_{CO_2}. Albedo is a mediator between the competing aerosol effects on the lightpath and their relative importance with respect to the direct lightpath since albedo controls the fraction of the incoming sunlight that contributes to the direct

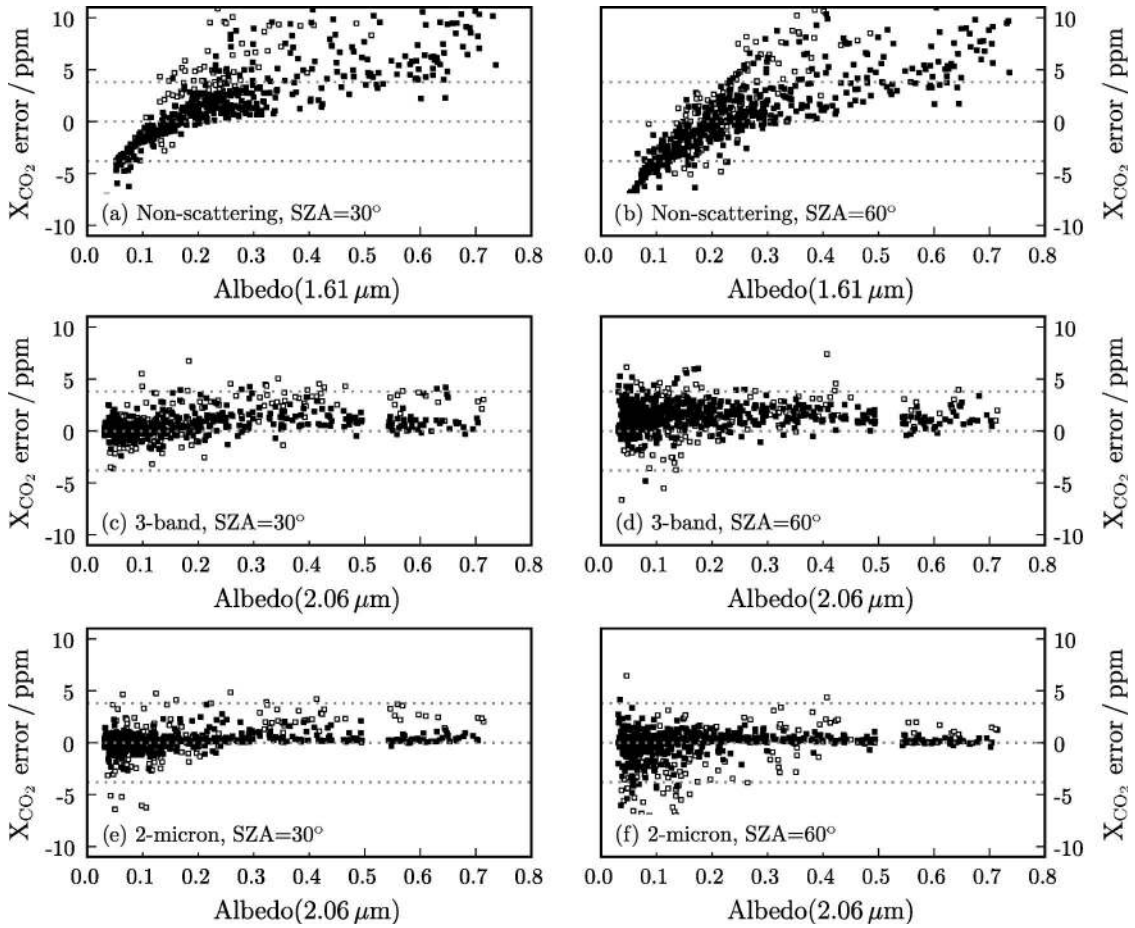

Fig. 9. Residual aerosol-induced X_{CO_2} error as a function of surface albedo at 1.61 or 2.06 μm for (a) and (b) "nonscattering" retrieval, (c) and (d) "3-band" retrieval, and (e) and (f) "2 micron" retrieval. Results are shown at SZA = 30° for (a), (c), and (e) and SZA = 60° for (b), (d), and (f). Filled and open boxes correspond to scenes with aerosol optical thickness less and greater than 0.3, respectively. Dotted gray lines indicate 1% error limits.

lightpath and that is available for further scattering processes after reflection at the surface.

The proposed "3-band" and "2 micron" retrievals confine the residual aerosol-induced retrieval error to less than 1% for most of the cases up to aerosol optical thickness 0.5 [Figs. 8(c)–8(f)]. The scatter among the retrieval errors increases with aerosol optical thickness and when going from SZA = 30° to SZA = 60°. For the "3-band" retrieval, overestimation of X_{CO_2} occurs in more cases than underestimation, which is in particular true for SZA = 60°. This pattern is not found for the "2 micron" retrieval, where the number of cases with high and low retrievals is balanced. For the "3-band" and "2 micron" retrievals, the residual X_{CO_2} error shows no pronounced dependence on surface albedo [Figs. 9(c)–9(f)]. The retrieval methods work almost equally well for all considered aerosol types parameterized through the Ångstrom coefficient [Figs. 10(c)–10(f)]. Tentatively, there is a correlation of larger retrieval errors with small Ångstrom coefficients. This pattern is less pronounced for the "2 micron" retrieval than for the "3-band" retrieval. In particular, the latter reveals enhanced retrieval errors for $\beta < 0.5$, which is not seen for the "2 micron" retrieval. We point out that, given a certain aerosol column number density, the aerosol optical thickness in the CO_2 bands and, hence, the overall aerosol impact on CO_2 retrievals is larger for small than for large Ångstrom coefficients.

The origin of the residual errors for the "3-band" and "2 micron" retrievals are the approximations incorporated into the retrieval forward model. In particular, this is the assumption that atmospheric aerosols and their height distribution can be described by a single type of aerosol characterized by the parameter α through a power-law size distribution, by the fixed-value aerosol refractive indices m_r and m_i, and by the parameter z_{aer} through a Gaussian height distribution of aerosol optical thickness. The aerosol-related state vector elements compensate for these approximations to some extent but a residual effect on retrieved CO_2 remains. Along this line, the retrieved aerosol parameters have to be regarded as effective parameters that compensate for all forward model approximations of the retrieval method.

Figure 11 summarizes our findings by showing the occurrence of X_{CO_2} retrieval errors among the discussed methods for our retrieval trials. Figure 11 aims at comparing the discussed retrieval methods

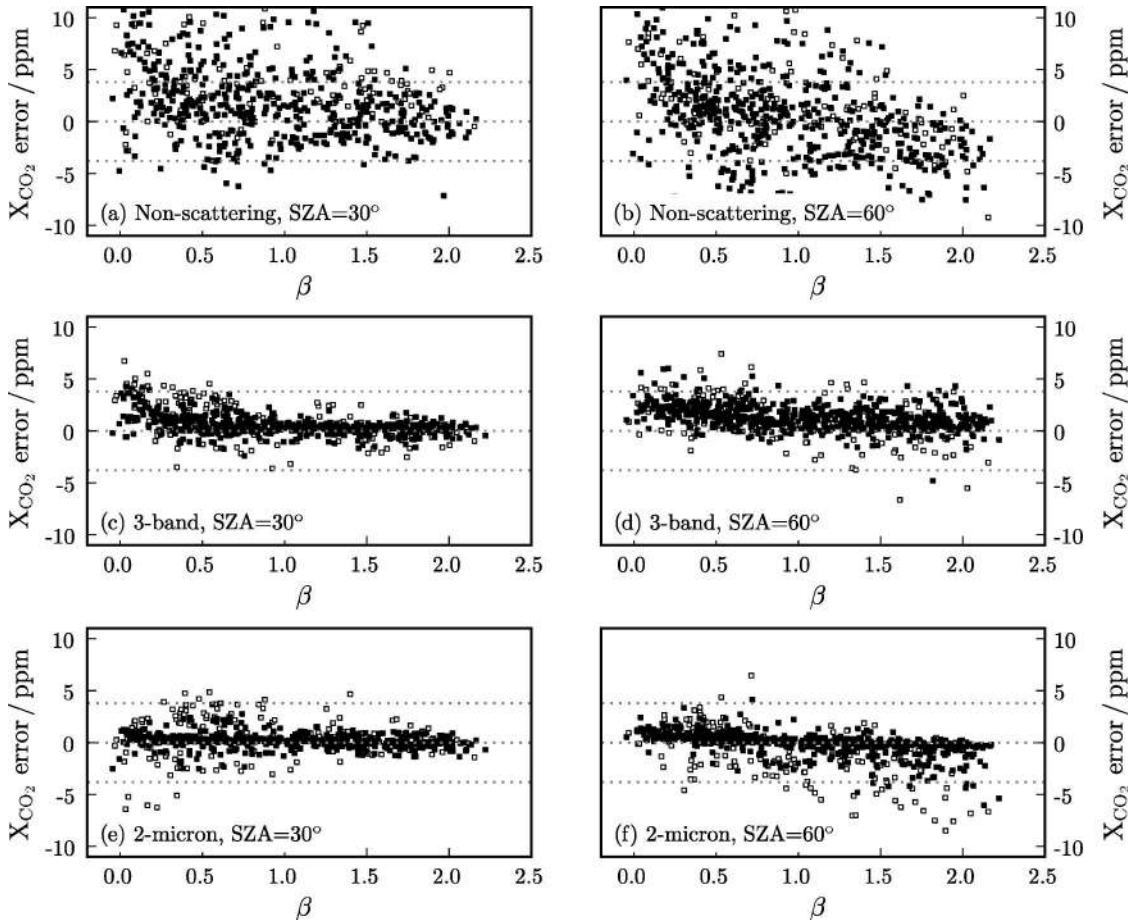

Fig. 10. Residual aerosol-induced X_{CO_2} error as a function of Ångstrom coefficient β for (a) and (b) "nonscattering" retrieval, (c) and (d) "3-band" retrieval, and (e) and (f) "2 micron" retrieval. Results are shown at SZA = 30° for (a), (c), and (e) and SZA = 60° for (b), (d), and (f). Filled and open boxes correspond to scenes with aerosol optical thickness less and greater than 0.3, respectively. Dotted gray lines indicate 1% error limits.

from a statistical point of view when applied to the same trial ensemble. We emphasize that our study and, in particular, Fig. 11 is not suited to conclude on-average residual X_{CO_2} errors or biases in a certain place at a certain time since the trial ensemble is not representative for such spatial and temporal averaging. The "2 micron" approach performs actually better than the "3-band" approach. In particular, the "2 micron" retrievals reveal less tendency to a positive bias than the "3-band" retrievals. While the median residual X_{CO_2} error of the "2 micron" retrievals (up to aerosol optical thickness 0.5) is well below 0.3 ppm for both SZA = 30° and SZA = 60°, the "3-band" retrievals yield median residual X_{CO_2} errors of 0.4 ppm and 1.2 ppm for SZA = 30° and SZA = 60°, respectively.

Comparing the proposed methods, the good performance of the "2 micron" approach might seem surprising since information on aerosols in the relatively narrow CO_2 absorption band around 2.06 μm is limited compared to the "3-band" retrieval range, which covers spectral bands between 0.77 and 2.06 μm including the O_2 A band commonly used for aerosol and cloud property retrievals. On the other hand, our goal here is to retrieve X_{CO_2} as accurately as possible not to retrieve aerosol properties. A particular advantage of the "2 micron" approach is the limited spectral variability of aerosol optical properties within the relatively narrow 2.06 μm band. From our ensemble simulations, it follows that aerosol amount and height can effectively account for erroneous assumptions about aerosol size and refractive index (and thus, phase function and single-scattering albedo). The "3-band" method faces the additional difficulty of dealing with the impact of aerosols on the measurements in a wide spectral range where spectral variability of aerosol optical properties is pronounced. An additional parameter representing aerosol size is retrievable to effectively account for this difficulty. Empirically, our retrieval trials show that both methods, the "3-band" and the "2 micron" method, can compensate for aerosol-induced errors on X_{CO_2} but that the "2 micron" method is tentatively better for error compensation.

Furthermore, the "2 micron"' approach might be an appealing choice in the view of possible instrument calibration errors. Since the "2 micron" retrieval by definition only uses a single retrieval window, it is not sensitive to inconsistencies of the radiance calibration among several retrieval windows. The

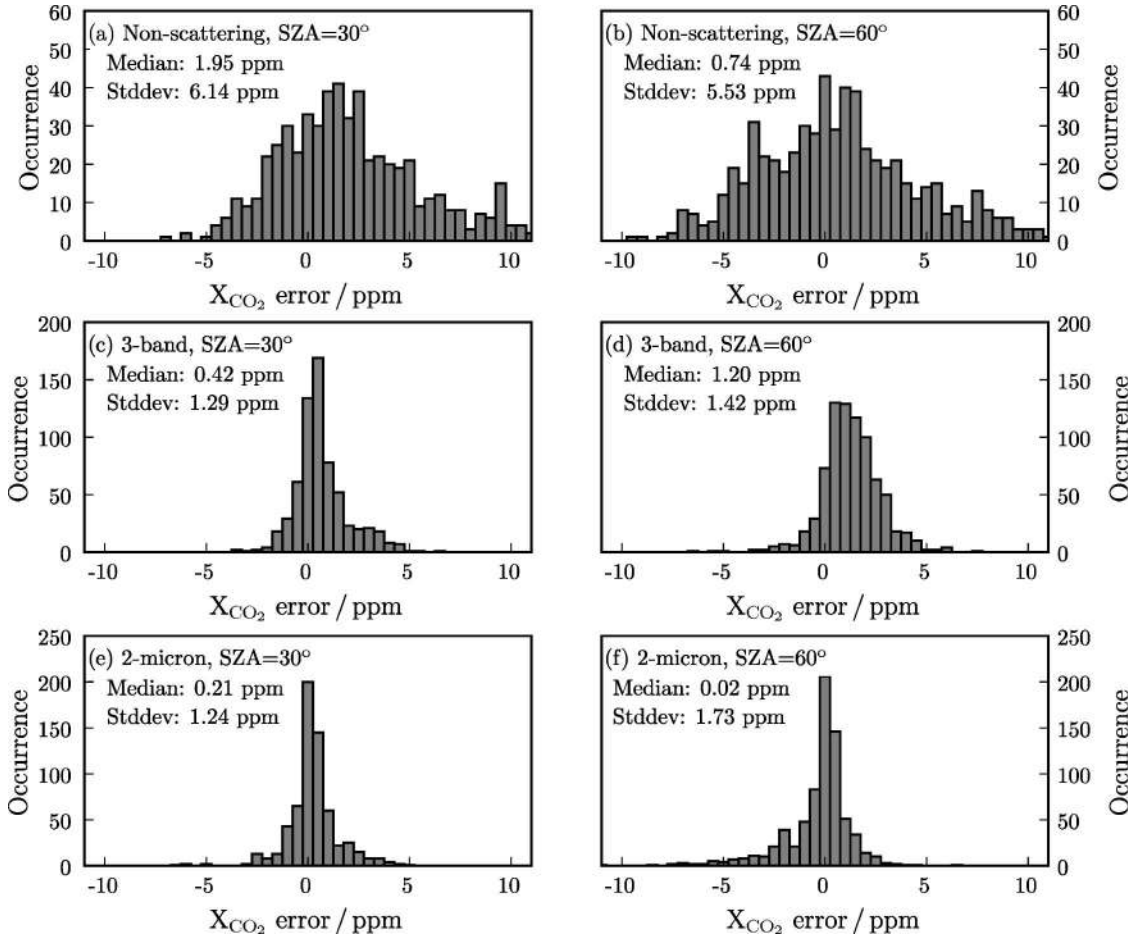

Fig. 11. Histograms of the residual aerosol-induced X_{CO_2} error for (a) and (b) "nonscattering" retrieval, (c) and (d) "3-band" retrieval, and (e) and (f) "2 micron" retrieval. Results are shown at SZA = 30° for (a), (c), and (e) and SZA = 60° for (b), (d), and (f). Median and standard deviation (Stddev) are given in each panel.

"3-band" method or any other retrieval method inferring aerosol properties from several spectral windows, however, relies on the assumption that the observed radiances are well interwindow calibrated, such that the spectral variability of aerosol effects is not masked by calibration errors. On the other hand, a retrieval approach that covers the 1.61 μm CO_2 absorption band in addition to the 2.06 μm band yields smaller noise errors since more measurements contribute to the retrieval of the CO_2 total column. Further, it might be found that the accuracy of meteorological support data is insufficient and that meteorological properties of the ambient atmosphere, such as surface pressure, are preferably retrieved from the measurements themselves [18]. Then, a retrieval covering several spectral bands, in particular covering the O_2 A band, is likely superior to a "2 micron"-type approach.

When assessing the importance of the residual X_{CO_2} retrieval errors for determination of CO_2 sources and sinks, the inferred error estimates have to be weighted by their actual occurrence probability in prospective satellite observations. To this end, the satellite sampling and observation strategy is to be related to the spatial and temporal distribution of surface scenes and aerosol occurrence. Then implications for inversion of CO_2 sources and sinks can be discussed taking into account averaging effects when assimilating the satellite data into a source-sink inverse model [7,9,10].

B. Generic Cirrus Retrievals

The proposed retrieval approaches are also applied to the trial ensemble containing cirrus clouds. Figure 12 shows the residual aerosol and cirrus-induced X_{CO_2} error as a function of surface albedo for the "nonscattering" retrieval and as a function of particulate optical thickness ($\tau_{aer,s} + \tau_{cir,s}$) for the "3-band" and "2 micron" retrievals. Interpretation of Fig. 12 is not as straightforward as for Figs. 8–10, since the cirrus trial spectra are simulated assuming a single type of generic cirrus cloud with optical thickness 0.1 confined to a layer between 9 and 10 km height, i.e., no ensemble of cirrus properties is considered. Hence, the choice of the generic cirrus cloud properties can generate a systematic pattern of the residual X_{CO_2} errors, which could appear random in a

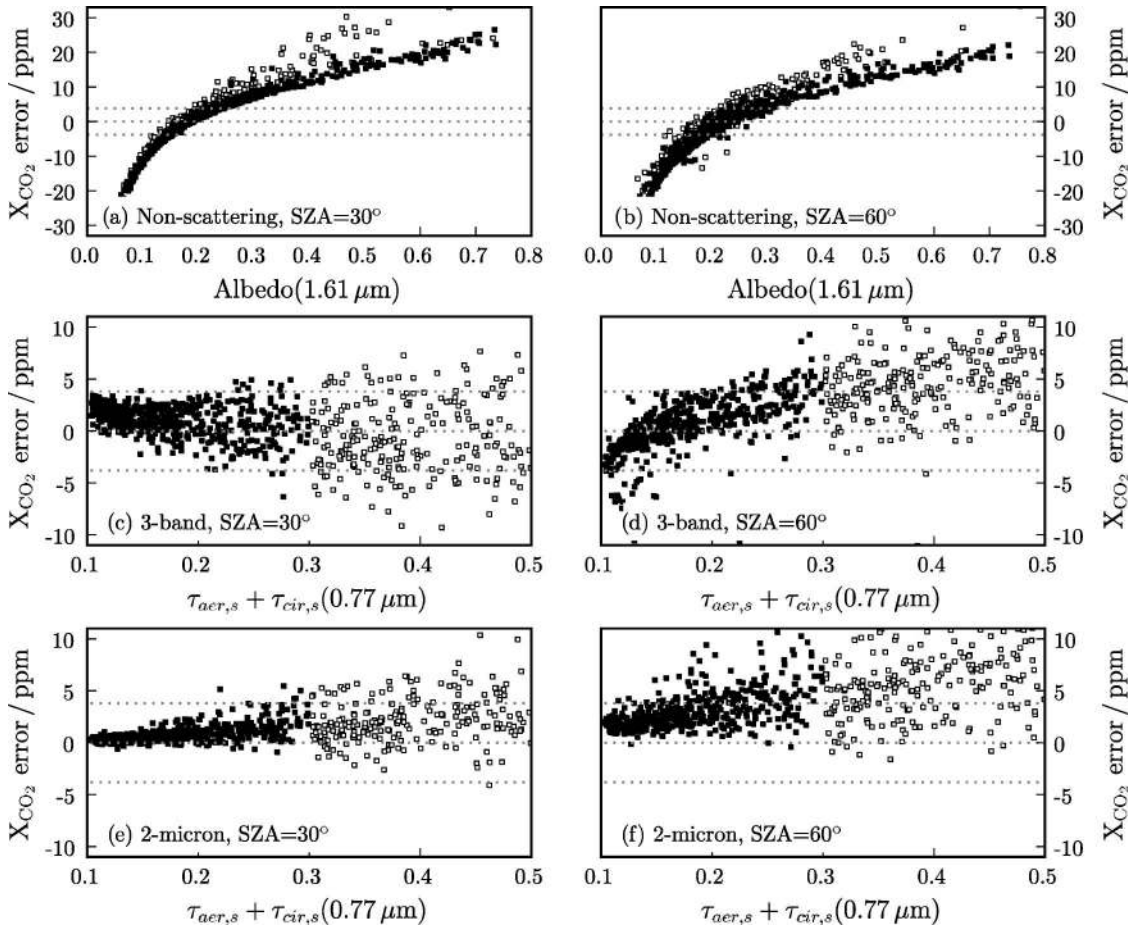

Fig. 12. Residual aerosol and cirrus induced X_{CO_2} error as a function of albedo at 1.61 μm for the (a) and (b) "nonscattering" retrieval and as a function of particulate optical thickness ($\tau_{aer,s} + \tau_{cir,s}$) at 0.77 μm for (c) and (d) "3-band" retrieval and (e) and (f) "2 micron" retrieval. Results are shown at SZA = 30° for (a), (c), and (e) and SZA = 60° for (b), (d), and (f). Filled and open boxes correspond to scenes with particulate optical thickness less and greater than 0.3, respectively. Dotted gray lines indicate 1% error limits. Note the extended ordinate scale in (a) and (b).

climatological ensemble of cirrus properties. Nevertheless, we regard our cirrus trials as examples of how well the proposed methods can perform under cirrus-loaded conditions.

Errors of the "nonscattering" retrieval are as high as 30 ppm [Figs. 12(a) and 12(b)] exceeding the errors found for aerosol-only scenes. The large effect of cirrus clouds on the CO_2 retrievals is due to their occurrence at high altitudes and due to cirrus optical thickness showing no decrease for increasing wavelengths in the near infrared. Hence, cirrus scattering events are very effective in shortening or enhancing the lightpath, and the overall scattering probability in the CO_2 bands is high. The residual retrieval error for the "nonscattering" retrieval strongly depends on surface albedo. There is an overall lightpath-shortening effect for low albedo and an overall lightpath-enhancing effect for high albedo with a net vanishing effect for albedo $\sim$0.2 (at 1.61 μm). Evidently, this correlation is less tight when considering multiple types and height distributions of cirrus clouds.

The "3-band" and "2 micron" approaches are able to account for the effect of cirrus clouds on CO_2 retrievals to a large extent [Figs. 12(c)–12(f)]. For SZA = 30°, residual retrieval errors are within 1% up to particulate optical thickness 0.3 with a tendency to overestimate X_{CO_2}. In particular, the "2 micron" retrieval reveals small retrieval errors for moderate particulate optical thickness. For SZA = 60°, retrieval performance is generally worse, although retrieval errors are again mostly below 1% up to particulate optical thickness 0.3. For the cirrus representation adopted here, the "3-band" retrievals show a dependence on particulate optical thickness with an underestimation of X_{CO_2} for pure cirrus cases and an overestimation of X_{CO_2} for cases with significant contribution from aerosols. The "2 micron" retrievals are biased towards high X_{CO_2} for most of the cases, and the scatter increases substantially with particulate optical thickness.

Compared to the aerosol-only trials, the spread of the residual X_{CO_2} retrieval errors increases considerably when adding the generic cirrus cloud. For $\tau_{aer,s} + \tau_{cir,s} > 0.3$ errors can exceed 1%. In addition to the error sources discussed for the aerosol-only retrieval trials, the residual X_{CO_2} retrieval errors for the cirrus containing ensemble originate from the fundamental difference between the ensemble simulations and the retrieval forward model in calculating particle optical properties. The simulations use the cirrus cloud model described in Subsection 3.B to model cirrus optical properties. The retrieval methods, however, try to model cirrus effects by the approximate aerosol retrieval model, which relies on Mie theory and fundamentally differs from the cirrus cloud model by the underlying physics approach. This inconsistency results in an additional contribution to the residual X_{CO_2} error. Further, adopting a cirrus cloud between 9 and 10 km, in addition to the atmospheric aerosol burden, renders the height distribution of scatterers for the cirrus ensemble more complex than for the aerosol-only ensemble.

Evidently, cirrus cloud effects remain the dominant source of uncertainty for X_{CO_2} retrievals by the proposed retrieval methods. Partially, this is due to the design of the methods being dedicated to account primarily for aerosol-only effects. Future improvements of the methods will focus on retrieval performance for cirrus-loaded scenes.

5. Conclusions

We discuss two implementations of a retrieval approach that accounts for the effect of atmospheric scatterers on retrievals of X_{CO_2} from spaceborne measurements of backscattered near-infrared sunlight. The approach is based on an effective parameterization of aerosol amount, aerosol height distribution, and aerosol microphysical properties. Effective aerosol parameters are inferred simultaneously with the CO_2 total column. The "3-band" implementation exploits the molecular absorption bands of O_2 around 0.77 μm and of CO_2 around 1.61 μm and 2.06 μm. Retrieved aerosol parameters are the column number density of particles, a single parameter characterizing the center height and width of a Gaussian aerosol height distribution, and the power of a power-law aerosol size distribution. The latter parameter effectively models the dependence of aerosol optical properties on wavelength. The "2 micron" implementation uses the CO_2 absorption band around 2.06 μm, only. Retrieved aerosol parameters are the column number density of particles, and a single parameter characterizing the center height and width of a Gaussian aerosol height distribution. The proposed methods are tested for a trial ensemble of simulated observations of a nadir sounder that measures the considered spectral bands at high spectral resolution over land surfaces. Ocean and snow covered surfaces are not considered. The simulations adopt aerosol loaded conditions from the global aerosol model ECHAM5-HAM. In addition, retrieval performance is tested for scenes with cirrus cloud cover of optical thickness 0.1.

Applying the retrieval methods to the trial ensemble yields residual aerosol-induced X_{CO_2} errors mostly below 1% up to aerosol optical thickness 0.5. Residual retrieval errors are largely independent of surface albedo and aerosol type. Observations at SZA = 60° are more challenging than observations at SZA = 30°. In general, the "2 micron" retrievals yield smaller residual errors than the "3-band" retrievals. The latter reveal a tendency to overestimate X_{CO_2}. The "2 micron" approach seems a promising alternative method to accurately retrieve atmosperic CO_2 abundances under aerosol (and cirrus) loaded conditions in a simple observational setup. Overlaying the aerosol with a cirrus cloud of optical thickness 0.1 enhances residual retrieval errors. Yet, errors are mostly below 1% for particulate optical thickness up to 0.3.

The proposed methods are applicable to GOSAT and OCO-like satellite missions, with GOSAT potentially providing the first real measurements. Thereby, observations of the TANSO-FTS onboard GOSAT bear the potential for refining the proposed approach by exploiting the polarization measurement capabilities and the broad spectral coverage of the instrument.

Part of this research was supported by the Dutch User Support Programme 2001-2005 under project GO-2005/064. The cirrus cloud model is a courtesy of the Royal Dutch Meteorological Institute (KNMI) through Wouter Knap. ECHAM5-HAM model output is provided by Gerrit de Leeuw, Finish Meteorological Institute (FMI). MODIS data are distributed by the Land Processes Distributed Active Archive Center (LP DAAC), located at the U.S. Geological Survey (USGS) Earth Resources Observation and Science Center (EROS) [39].

References

1. T. Yokota, H. Oguma, I. Morino, A. Higurashi, T. Aoki, and G. Inoue, "Test measurements by a BBM of the nadir-looking SWIR FTS aboard GOSAT to monitor CO_2 column density from space," in *Society of Photo-Optical Instrumentation Engineers (SPIE) Conference Series*, S. C. Tsay, T. Yokota, and M.-H. Ahn, eds. (2004), Vol. 5652, pp, 182–188.
2. D. Crisp, R. M. Atlas, F.-M. Bréon, L. R. Brown, J. P. Burrows, P. Ciais, B. J. Connor, S. C. Doney, I. Y. Fung, D. J. Jacob, C. E. Miller, D. O'Brien, S. Pawson, J. T. Randerson, P. Rayner, R. J. Salawitch, S. P. Sander, B. Sen, G. L. Stephens, P. P. Tans, G. C. Toon, P. O. Wennberg, S. C. Wofsy, Y. L. Yung, Z. Kuang, B. Chudasama, G. Sprague, B. Weiss, R. Pollock, D. Kenyon, and S. Schroll, "The Orbiting Carbon Observatory (OCO) mission," Adv. Space Res. **34**, 700–709 (2004).
3. Z. Kuang, J. Margolis, G. Toon, D. Crisp, and Y. Yung, "Spaceborne measurements of atmospheric CO_2 by high-resolution NIR spectrometry of reflected sunlight: an introductory study," Geophys. Res. Lett. **29**, 1716–1720 (2002).
4. J. Mao and S. R. Kawa, "Sensitivity studies for space-based measurement of atmospheric total column carbon dioxide by reflected sunlight," Appl. Opt. **43**, 914–927 (2004).
5. P. J. Rayner and D. M. O'Brien, "The utility of remotely sensed CO_2 concentration data in surface source inversions," Geophys. Res. Lett. **28**, 175–178 (2001).
6. S. Houweling, F.-M. Bréon, I. Aben, C. Rödenbeck, M. Gloor, M. Heimann, and P. Ciais, "Inverse modeling of CO_2 sources and sinks using satellite data: a synthetic inter-comparison of measurement techniques and their performance as a function of space and time," Atmos. Chem. Phys. **4**, 523–538 (2004).
7. F. Chevallier, F.-M. Bréon, and P. J. Rayner, "Contribution of the Orbiting Carbon Observatory to the estimation of CO_2 sources and sinks: theoretical study in a variational data assimilation framework," J. Geophys. Res. **112**, D09307 (2007).
8. C. E. Miller, D. Crisp, P. L. DeCola, S. C. Olsen, J. T. Randerson, A. M. Michalak, A. Alkhaled, P. Rayner, D. J. Jacob, P. Suntharalingam, D. B. A. Jones, A. S. Denning, M. E. Nicholls, S. C. Doney, S. Pawson, H. Bösch, B. J. Connor, I. Y. Fung, D. O'Brien, R. J. Salawitch, S. P. Sander, B. Sen, P. Tans, G. C. Toon, P. O. Wennberg, S. C. Wofsy, Y. L. Yung, and R. M. Law, "Precision requirements for space-based X_{CO_2} data," J. Geophys. Res. **112**, D10314 (2007).
9. D. F. Baker, H. Bösch, S. C. Doney, and D. S. Schimel, "Carbon source/sink information provided by column CO_2 measurements from the Orbiting Carbon Observatory," Atmos. Chem. Phys. Disc. **8**, 20051–20112 (2008).
10. L. Feng, P. I. Palmer, H. Bösch, and S. Dance, "Estimating surface CO_2 fluxes from space-borne CO_2 dry air mole fraction observations using an ensemble Kalman Filter," Atmos. Chem. Phys. **9**, 2619–2633 (2008).
11. D. M. O'Brien and P. J. Rayner, "Global observations of the carbon budget 2. CO_2 column from differential absorption of reflected sunlight in the 1.61 μm band of CO_2," J. Geophys. Res. **107**, 4354 (2002).
12. E. Dufour and F.-M. Bréon, "Spaceborne estimate of atmospheric CO_2 column by use of the differential absorption method: error analysis," Appl. Opt. **42**, 3595–3609 (2003).
13. S. Houweling, W. Hartmann, I. Aben, H. Schrijver, J. Skidmore, G.-J. Roelofs, and F.-M. Bréon, "Evidence of systematic errors in SCIAMACHY-observed CO_2 due to aerosols," Atmos. Chem. Phys. **5**, 3003–3013 (2005).
14. I. Aben, O. Hasekamp, and W. Hartmann, "Uncertainties in the space-based measurements of CO_2 columns due to scattering in the Earth's atmosphere," J. Quant. Spectrosc. Radiat. Transfer **104**, 450–459 (2007).
15. H. Bösch, G. C. Toon, B. Sen, R. A. Washenfelder, P. O. Wennberg, M. Buchwitz, R. de Beek, J. P. Burrows, D. Crisp, M. Christi, B. J. Connor, V. Natraj, and Y. L. Yung, "Space-based near-infrared CO_2 measurements: testing the Orbiting Carbon Observatory retrieval algorithm and validation concept using SCIAMACHY observations over Park Falls, Wisconsin," J. Geophys. Res. **111**, D23302 (2006).
16. M. P. Barkley, P. S. Monks, A. J. Hewitt, T. Machida, A. Desai, N. Vinnichenko, T. Nakazawa, M. Y. Arshinov, N. Fedoseev, and T. Watai, "Assessing the near surface sensitivity of SCIAMACHY atmospheric CO_2 retrieved using (FSI) WFM-DOAS," Atmos. Chem. Phys. **7**, 3597–3619 (2007).
17. O. Schneising, M. Buchwitz, J. P. Burrows, H. Bovensmann, M. Reuter, J. Notholt, R. Macatangay, and T. Warneke, "Three years of greenhouse gas column-averaged dry air mole fractions retrieved from satellite Part 1: carbon dioxide," Atmos. Chem. Phys. **8**, 3827–3853 (2008).
18. B. J. Connor, H. Bösch, G. Toon, B. Sen, C. Miller, and D. Crisp, "Orbiting Carbon Observatory: inverse method and prospective error analysis," J. Geophys. Res. **113**, D05305 (2008).
19. S. Oshchepkov, A. Bril, and T. Yokota, "PPDF-based method to account for atmospheric light scattering in observations of carbon dioxide from space," J. Geophys. Res. **113**, D23210 (2008).
20. O. P. Hasekamp and J. Landgraf, "A linearized vector radiative transfer model for atmospheric trace gas retrieval," J. Quant. Spectrosc. Radiat. Transfer **75**, 221–238 (2002).
21. O. P. Hasekamp and J. Landgraf, "Linearization of vector radiative transfer with respect to aerosol properties and its use in satellite remote sensing," J. Geophys. Res. **110**, D04203 (2005).
22. O. P. Hasekamp and J. Landgraf, "Retrieval of aerosol properties over the ocean from multispectral single-viewing-angle measurements of intensity and polarization: retrieval approach, information content, and sensitivity study," J. Geophys. Res. **110**, D20207 (2005).
23. B. van Diedenhoven, O. P. Hasekamp, and J. Landgraf, "Retrieval of cloud parameters from satellite-based reflectance measurements in the ultraviolet and the oxygen A-band," J. Geophys. Res. **112**, D15208 (2007).
24. O. P. Hasekamp and A. Butz, "Efficient calculation of intensity and polarization spectra in vertically inhomogeneous scattering and absorbing atmospheres," J. Geophys. Res. **113**, D20309 (2008).
25. L. S. Rothman, D. Jacquemart, A. Barbe, D. Chris Benner, M. Birk, L. R. Brown, M. R. Carleer, C. Chackerian, K. Chance, L. H. Coudert, V. Dana, V. M. Devi, J.-M. Flaud,

R. R. Gamache, A. Goldman, J.-M. Hartmann, K. W. Jucks, A. G. Maki, J.-Y. Mandin, S. T. Massie, J. Orphal, A. Perrin, C. P. Rinsland, M. A. H. Smith, J. Tennyson, R. N. Tolchenov, R. A. Toth, J. Vander Auwera, P. Varanasi, and G. Wagner, "The HITRAN 2004 molecular spectroscopic database," J. Quant. Spectrosc. Radiat. Transfer **96**, 139–204 (2005).
26. R. A. Toth, L. R. Brown, C. E. Miller, V. Malathy Devi, and D. C. Benner, "Spectroscopic database of CO_2 line parameters: 4300 7000 cm^{-1}," J. Quant. Spectrosc. Radiat. Transfer **109**, 906–921 (2008).
27. H. C. van de Hulst, *Light Scattering by Small Particles* (John Wiley & Sons, 1957).
28. W. A. de Rooij and C. C. A. H. van der Stap, "Expansion of Mie scattering matrices in generalized spherical functions," Astron. Astrophys. **131**, 237–248 (1984).
29. M. I. Mishchenko, I. V. Geogdzhayev, B. Cairns, W. B. Rossow, and A. A. Lacis, "Aerosol retrievals over the ocean by use of channels 1 and 2 AVHRR data: sensitivity analysis and preliminary results," Appl. Opt. **38**, 7325–7341 (1999).
30. J. E. Hansen and L. D. Travis, "Light scattering in planetary atmospheres," Space Sci. Rev. **16**, 527–610 (1974).
31. O. Dubovik, B. N. Holben, T. F. Eck, A. Smirnov, Y. J. Kaufman, M. D. King, D. Tanré, and I. Slutsker, "Variability of absorption and optical properties of key aerosol types observed in worldwide locations," J. Atmos. Sci. **59**, 590–608 (2002).
32. P. Stier, J. Feichter, S. Kinne, S. Kloster, E. Vignati, J. Wilson, L. Ganzeveld, I. Tegen, M. Werner, Y. Balkanski, M. Schulz, O. Boucher, A. Minikin, and A. Petzold, "The aerosol-climate model ECHAM5-HAM," Atmos. Chem. Phys. **5**, 1125–1156 (2005).
33. Intergovernmental Panel on Climate Change (IPCC), Climate change 2007: the physical science basis. Contribution of Working Group I to the Fourth Assessment Report of the Intergovernmental Panel on Climate Change (2007).
34. M. Hess and M. Wiegner, "COP: a data library of optical properties of hexagonal ice crystals," Appl. Opt. **33**, 7740–7746 (1994).
35. M. Hess, "Scattering matrices of imperfect hexagonal ice crystals," J. Quant. Spectrosc. Radiat. Transfer **60**, 301–308 (1998).
36. A. J. Heymsfield and C. M. R. Platt, "A parameterization of the particle size spectrum of ice clouds in terms of the ambient temperature and the ice water content," J. Atmos. Sci. **41**, 846–855 (1984).
37. C. D. Rodgers, *Inverse Methods for Atmospheric Sounding: Theory and Practice* (World Scientific, 2000).
38. A. Bril, S. Oshchepkov, T. Yokota, and G. Inoue, "Parameterization of aerosol and cirrus cloud effects on reflected sunlight spectra measured from space: application of the equivalence theorem," Appl. Opt. **46**, 2460–2470 (2007).
39. URL:http://LPDAAC.usgs.gov